Supporting Information for:

Agar Aerogel Containing Small-Sized Zeolitic Imidazolate Framework Loaded Carbon Nitride: A Solar-Triggered Regenerable Decontaminant for Convenient and Enhanced Water Purification

Wentao Zhang,[†] Shuo Shi,[‡] Wenxin Zhu,[†] Lunjie Huang,[†] Chengyuan Yang,[†] Sihang Li,[†] Xinnan Liu,[†] Rong Wang,[†] Na Hu,[§] Yourui Suo,[§] Zhonghong Li,[†] Jianlong Wang*,[†]

Number of pages: 25

Number of figures: 19

Number of Tables: 04

Supporting Figures:

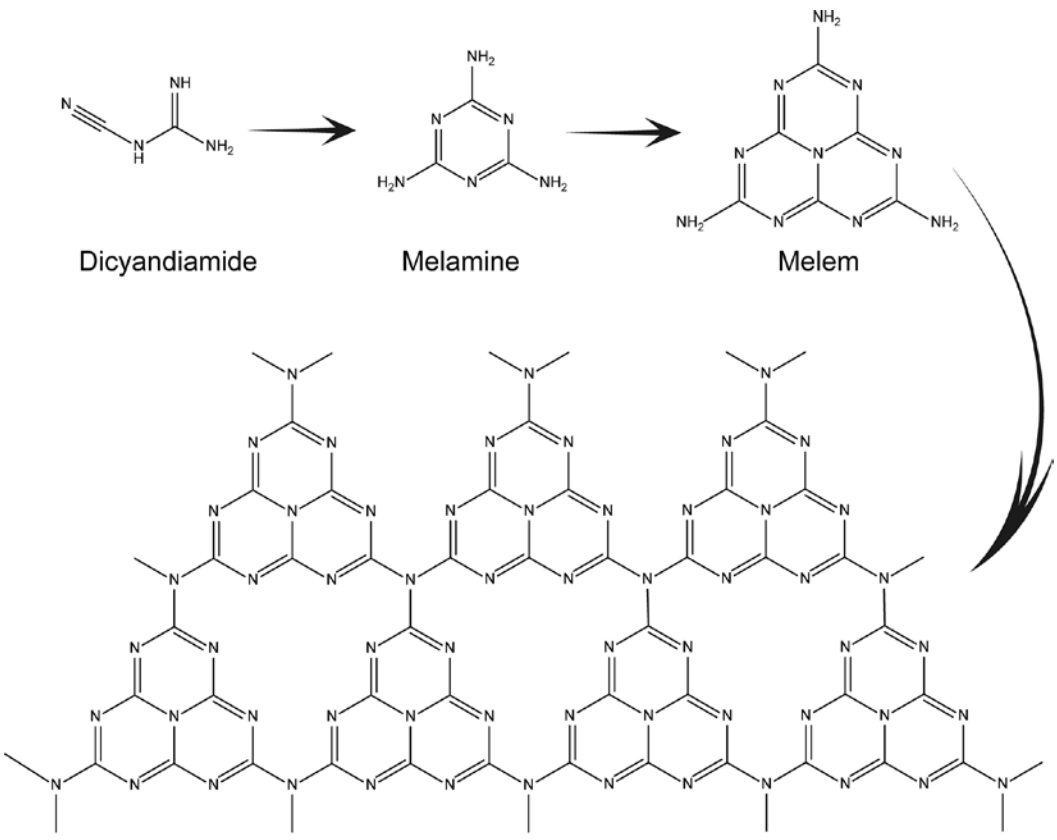

Figure S1. Reaction path for the formation of C_3N_4 from dicyandiamide.

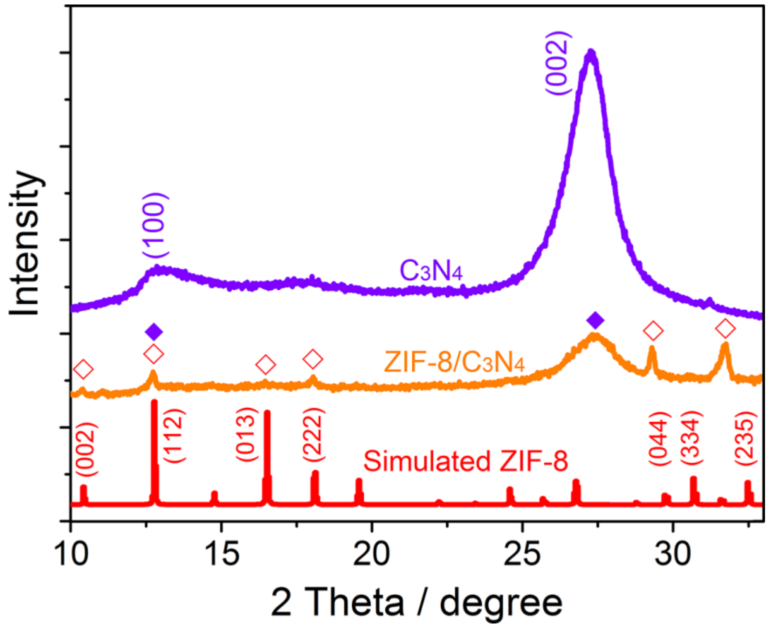

Figure S2. XRD patterns of C_3N_4, simulated ZIF-8 and the as-obtained ZIF-8/C_3N_4.

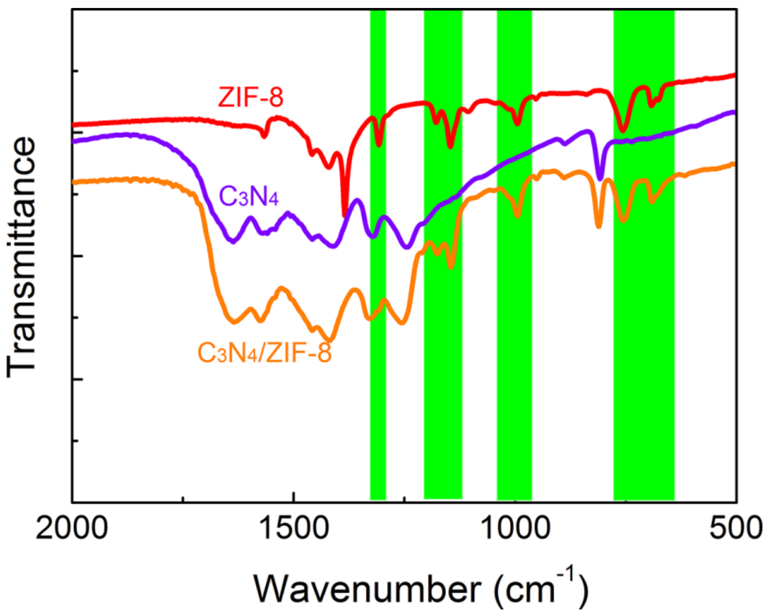

Figure S3. FT-IR spectra of C_3N_4, ZIF-8 and the as-obtained ZIF-8/C_3N_4.

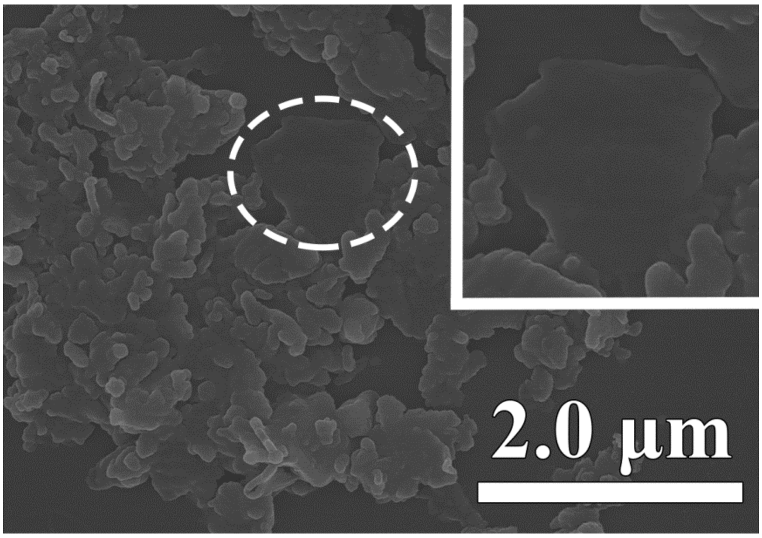

Figure S4. SEM image of C_3N_4 nanosheets.

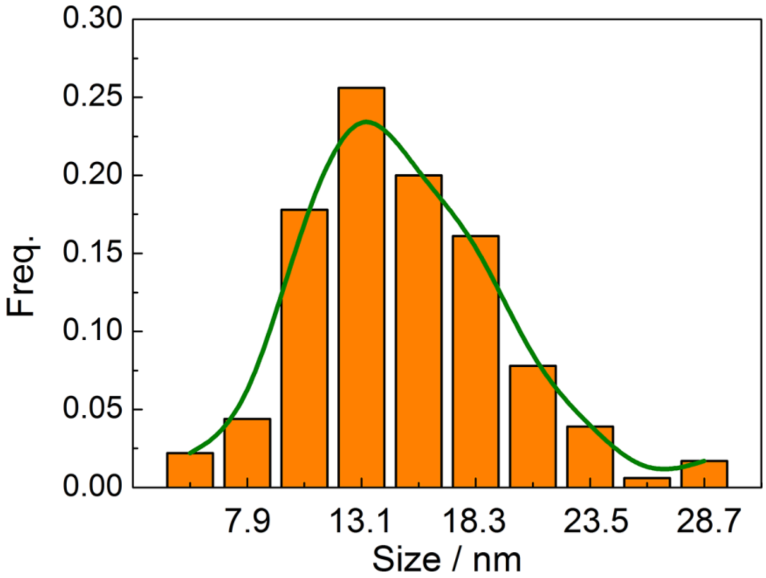

Figure S5. The size distribution of ZIF-8 nanoparticles on C_3N_4, over 150 particles were counted, indicating ZIF-8 nanoparticles possess average particle size, about 14.95 nm.

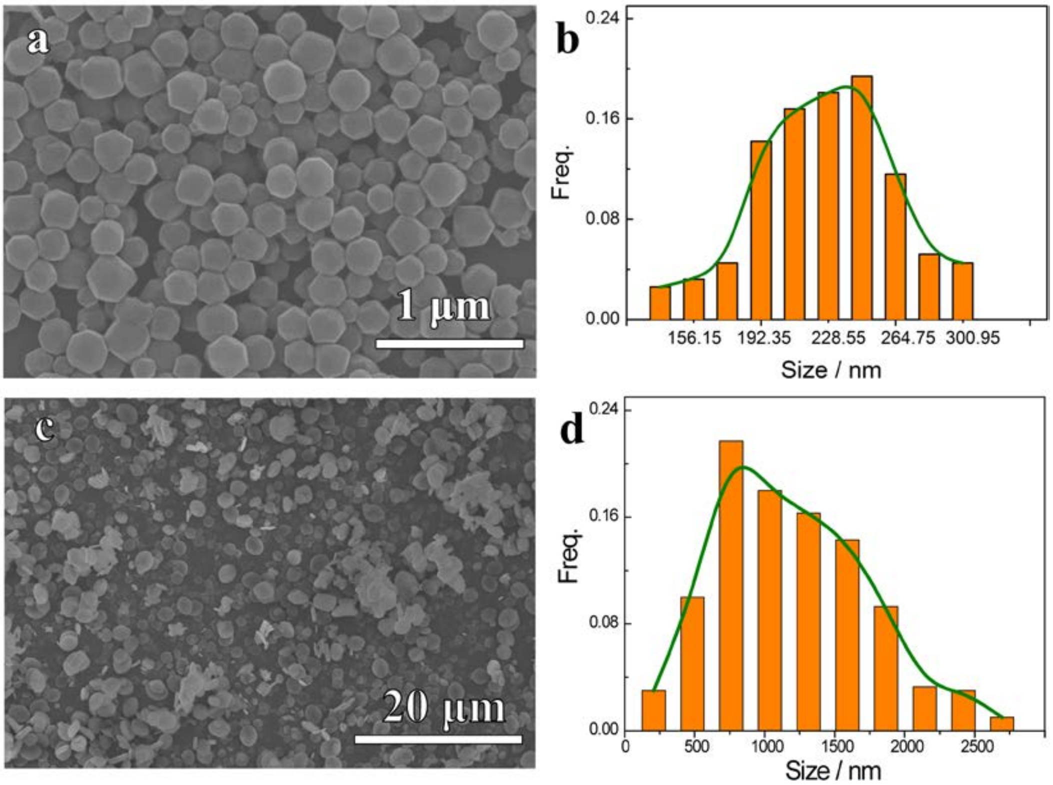

Figure S6. SEM image and size distribution of big-sized bulk ZIF-8, over 150 particles were counted. a, b) ZIF-8 nanoparticles, synthesized by a reported method,[1] possess average particle size of 227.61 nm. c,d) ZIF-8 nanoparticles with size of 1193.20 nm were synthesized by the same condition for ZIF-8/C_3N_4 but without the presence of C_3N_4.

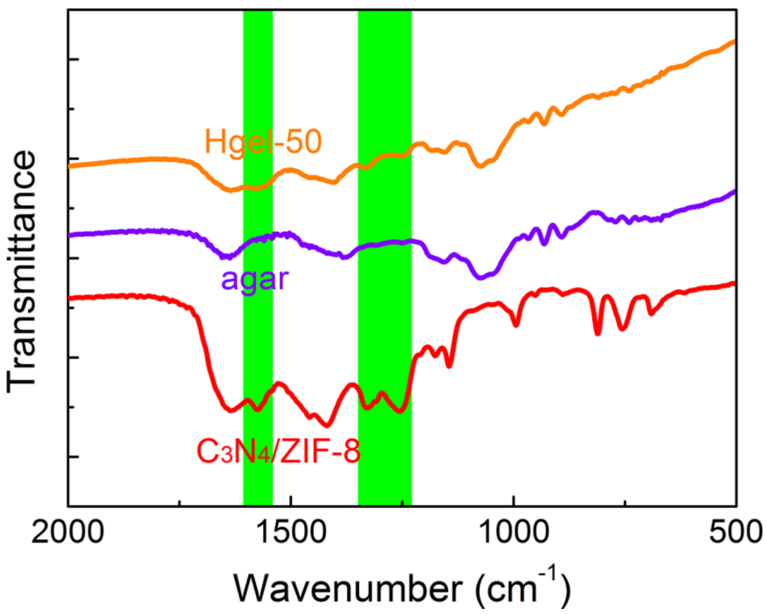

Figure S7. FT-IR spectra of agar, ZIF-8, C_3N_4 and Hgel-50.

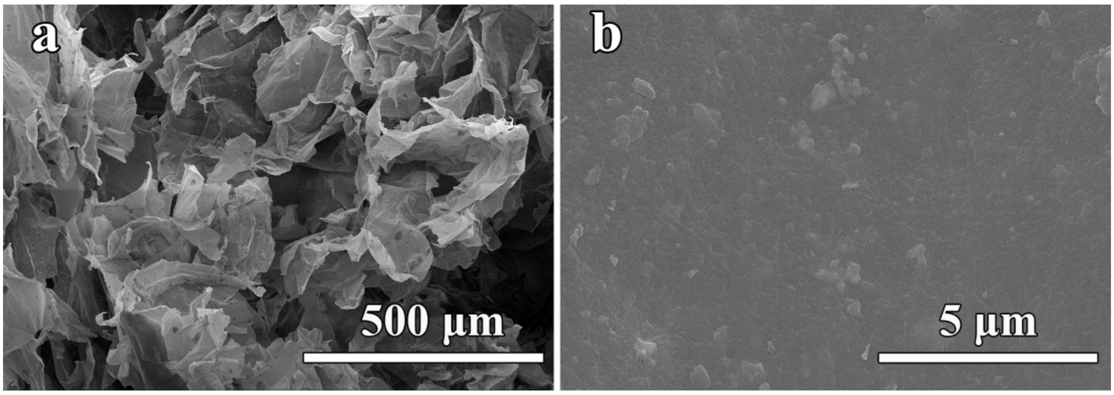

Figure S8. SEM of the hybrid aerogel containing 11.1% ZIF-8/C_3N_4.

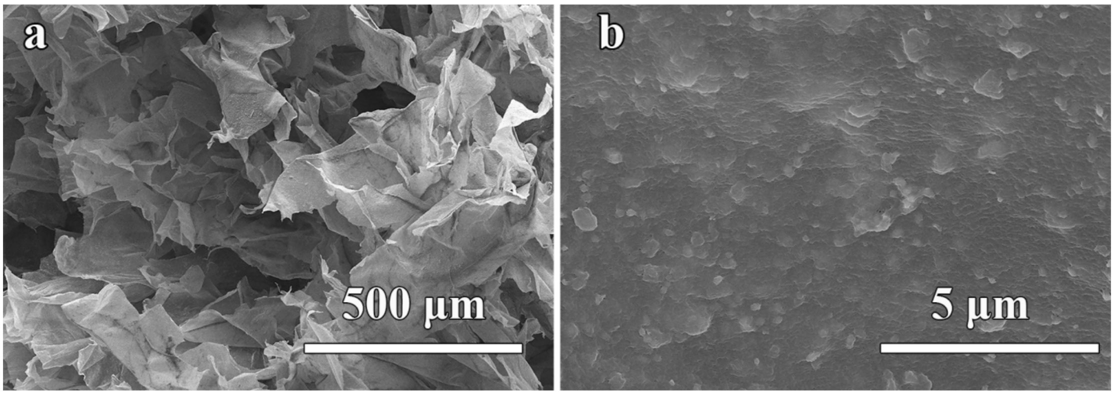

Figure S9. SEM of the hybrid aerogel containing 33.3% ZIF-8/C_3N_4.

Table S1. Adsorption capacities of various absorbents for Congo red.

Kind of adsorbent	Adsorption capacity Q_t [mg g^{-1}]	
	Detected[a)]	Simulated[b)]
Pure aerogel	8.23	-
C_3N_4	14.87	-
Big-sized bulk ZIF-8	789.73	-
ZIF-8/C_3N_4	504.42	352.71
11.1% ZIF-8/C_3N_4-aerogel	61.44	63.37
33.3% ZIF-8/C_3N_4-aerogel	178.63	173.46
50% ZIF-8/C_3N_4-aerogel	260.21	256.33

[a)]The data was the equilibrium absorption value in Figure 2b, which was conducted by soaking 5 mg acsorbent into 20 mL CR solution at 200 ppm over 10 h in a shaker; [b)]The simulated capacity of ZIF-8/C_3N_4 was calculated according to the proportions and data mesured for big-sized bulk ZIF-8 and C_3N_4; the capacity of three hybrid aerogel was calculated based on the mesured data for ZIF-8/C_3N_4 and Pure aerogel.

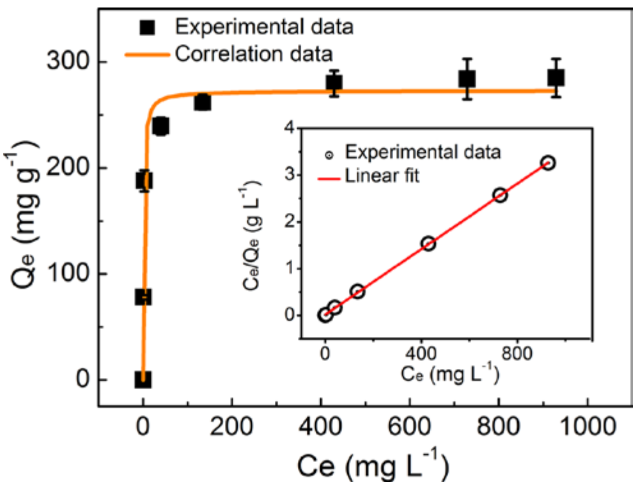

Figure S10. The adsorption isotherms of CR by Hgel-50 (correlation curve was drawn using the isotherm parameters calculated from the single-site adsorption isotherm model) and the linear fit of the model (inset).

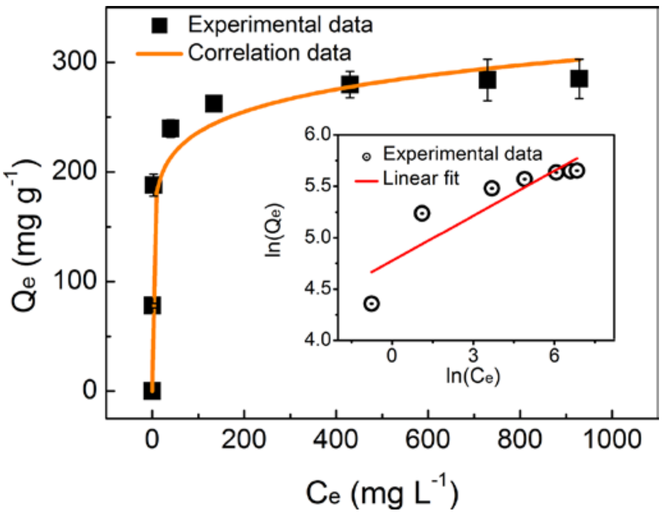

Figure S11. The adsorption isotherms of CR by Hgel-50 (correlation curve was drawn using the isotherm parameters calculated from the Freundlich isotherm model) and the linear fit of the model (inset).

Table S2. Thermodynamic parameters of Hgel-50 for CR adsorption.

	Single-site adsorption isotherm			Dual-site adsorption isotherm			Freundlich isotherm		
	Q_m (mg g^{-1})	K_L (L mg^{-1})	R^2	Q_m (mg g^{-1})	K_d (L mg^{-1})	R^2	K_F (mg g^{-1})	*1/n*	R^2
Hgel-50	272.87 ±6.11	0.76 ±0.14	0.985	287.35 ±5.77	1.10 ±0.07	0.995	141.56 ±18.17	0.11 ±0.02	0.929
Hgel-Z	190.13 ±3.75	0.14 ±0.02	0.989	208.75 ±1.55	0.24 ±0.02	0.997	82.79 ±11.82	0.13 ±0.03	0.942

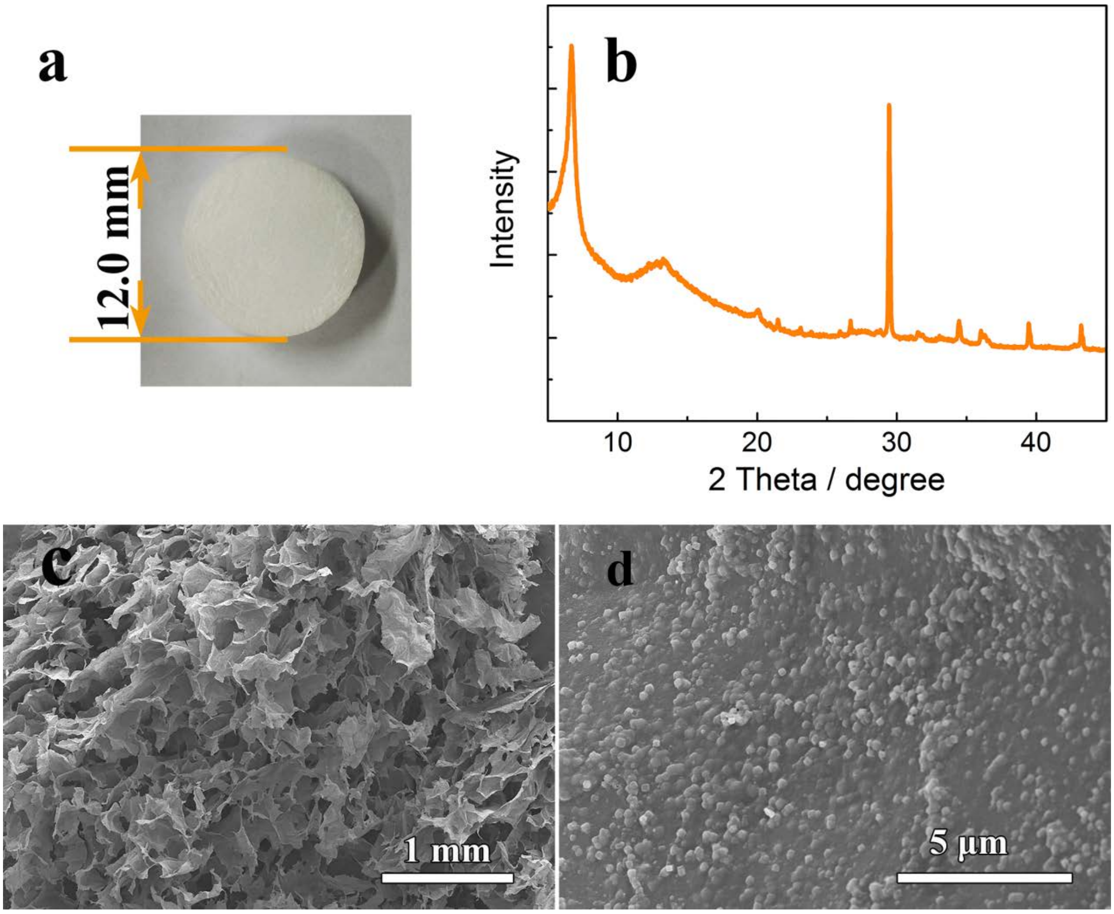

Figure S12. a) Photograph, b,c) SEM images and d) XRD pattern of aerogel containing 21.8% ZIF-8 (Hgel-Z).

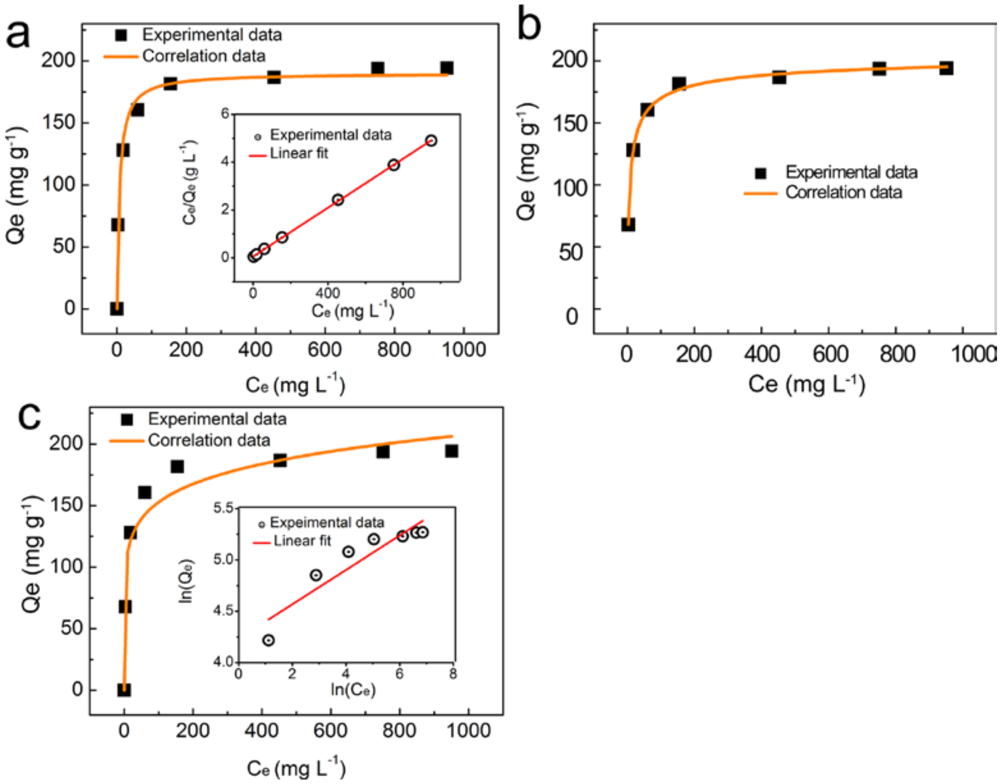

Figure S13. The single-site adsorption a), dual-site adsorption b) and Freundlich c) isotherm model for the adsorption isotherms of CR by Hgel-Z and the linear fit of the model (inset).

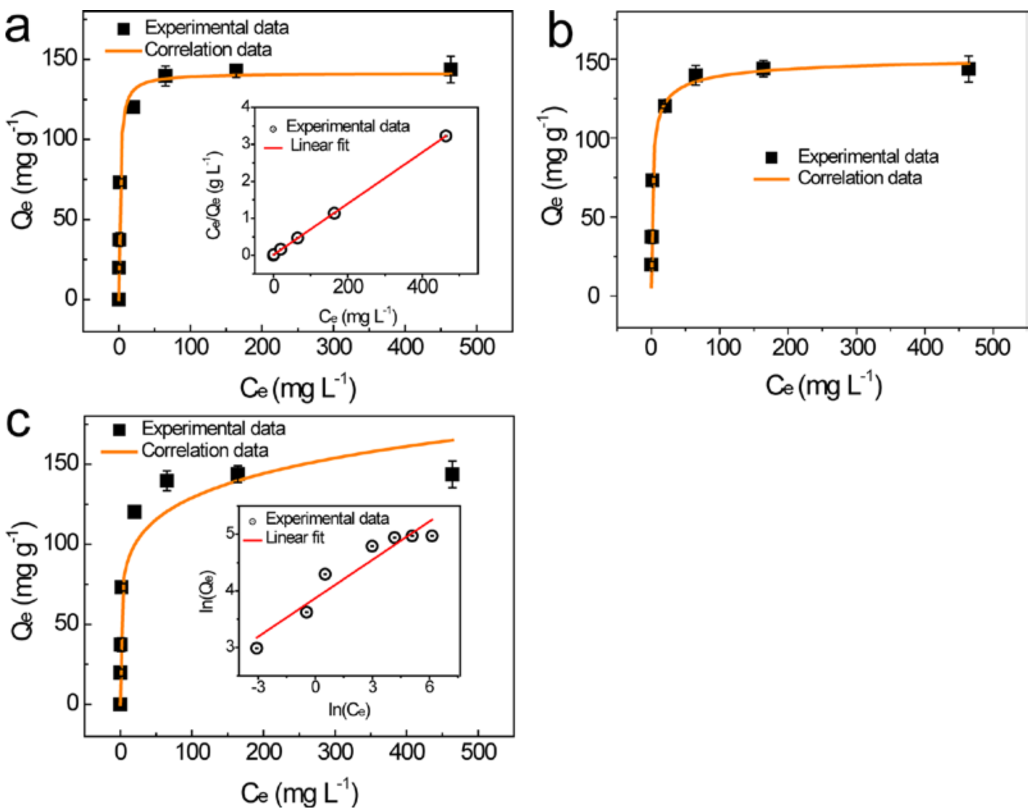

Figure S14. The single-site adsorption a), dual-site adsorption b) and Freundlich c) isotherm model for the adsorption isotherms of methylene blue by Hgel-50 and the linear fit of the model (inset).

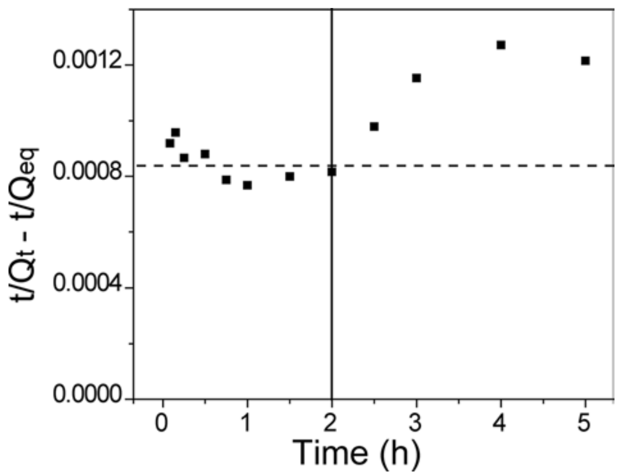

Figure S15. Invalidity of the pseudo-second-order conditions for the full time range of 5 hours.

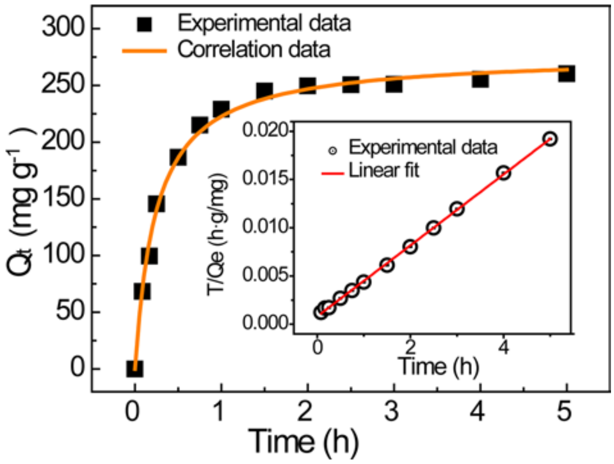

Figure S16. The adsorption kinetics of CR by Hgel-50 (correlation curve was drawn using the kinetic parameters calculated from the pseudo-second-order model of full time) and pseudo-second-order plots (inset).

Table S3. Adsorption kinetics parameters of Hgel-50 for CR adsorption.

	Pseudo-first-order			Pseudo-second-order of full times			Pseudo-second-order of lower times		
$Q_{e,exp}$ (mg g^{-1})	$Q_{e,c}$ (mg g^{-1})	k_1(h^{-1})	R^2	$Q_{e,c}$ (mg g^{-1})	$k_2\times10^{-2}$ (g mg h^{-1})	R^2	$Q_{e,c}$ (mg g^{-1})	$k_2\times10^{-2}$ (g mg h^{-1})	R^2
260.21	249.90 ±3.13	3.05 ±0.17	0.991	276.69 ±3.44	1.49 ±0.11	0.995	288.59 ±5.54	1.28 ±0.11	0.996

	Initial Phase			Secondary Phase		
Intraparticle diffusion model	K_{p1} (mg g^{-1} $h^{-0.5}$)	C_1	R^2	K_{p2} (mg g^{-1} $h^{-0.5}$)	C_1	R^2
	256.24±25.84	1.03±15.29	0.961	20.84±4.28	215.31±7.04	0.792

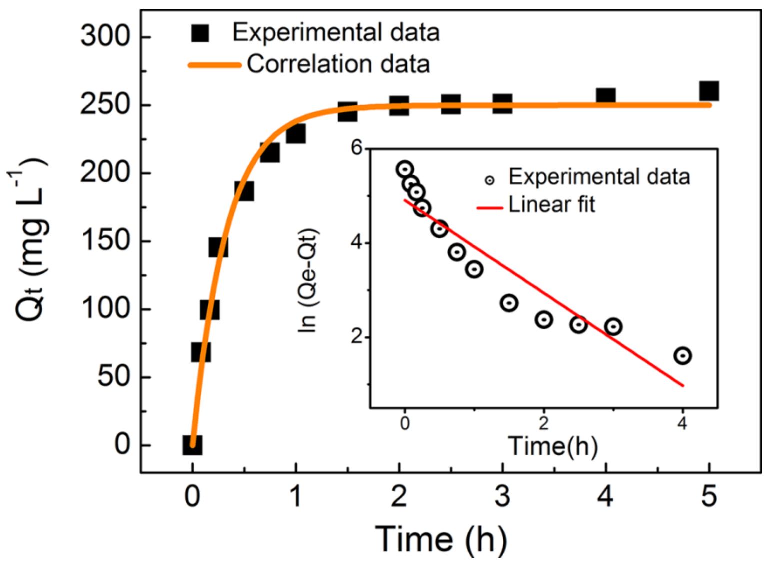

Figure S17. The adsorption kinetics of CR by Hgel-50 (correlation curve was drawn using the kinetic parameters calculated from the pseudo-first-order model of full time) and pseudo-first-order plots (inset).

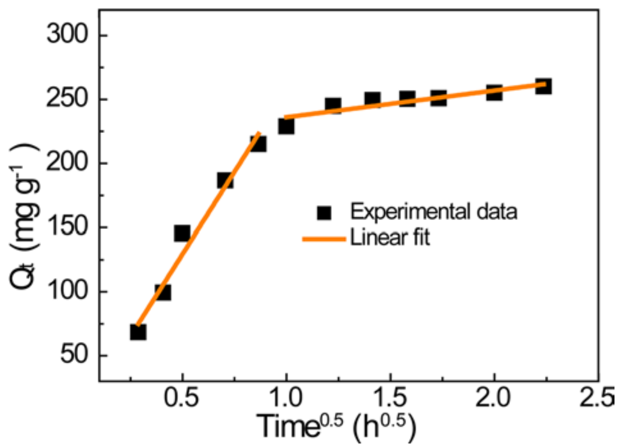

Figure S18. The intra-particle diffusion model for the adsorption of CR by Hgel-50.

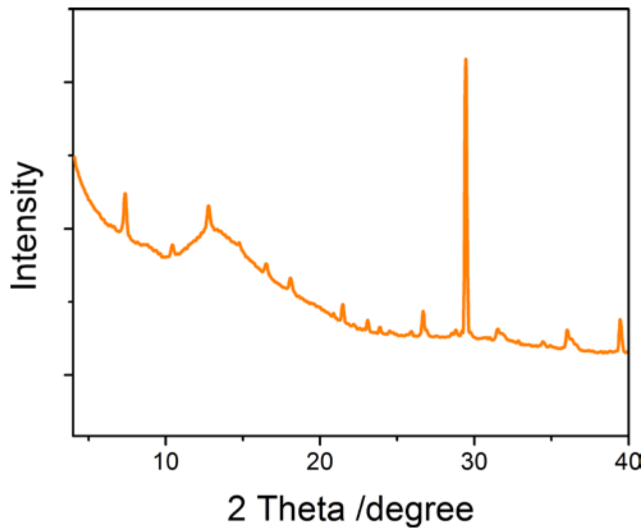

Figure S19. XRD pattern of the regenerated Hgel-50.

Table S4. Zn^{2+} concentration detected by atomic absorption spectrometer on pure water and water after treatment with Hgel-50.

	Pure water	CR solution after aerogel adsorption	CR solution after synergistic removal
Zn^{2+} concentration (ppm)	0.088±0.016	0.092±0.012	0.087±0.019

Reference

1. Torad, N. L.; Hu, M.; Kamachi, Y.; Takai, K.; Imura, M.; Naito, M.; Yamauchi, Y. Facile synthesis of nanoporous carbons with controlled particle sizes by direct carbonization of monodispersed ZIF-8 crystals. *Chem. Commun.* **2013,** *49* (25), 2521-2523.